

A NEW BESSE-TYPE RELAXATION SCHEME FOR THE NUMERICAL APPROXIMATION OF THE SCHRÖDINGER-POISSON SYSTEM

AGISSILAOS ATHANASSOULIS, THEODOROS KATSAOUNIS, IRENE KYZA, AND STEPHEN METCALFE

ABSTRACT. We introduce a new second order in time Besse-type relaxation scheme for approximating solutions of the Schrödinger-Poisson system. More specifically, we use the Crank-Nicolson scheme as a time stepping mechanism, the standard conforming finite element method for the spatial discretization whilst the nonlinearity is handled by means of a relaxation approach similar to the one introduced by Besse for the nonlinear Schrödinger equation [4]. We prove that discrete versions of the system's conservation laws hold and we conclude by presenting some numerical experiments, including an example from cosmology, that demonstrate the effectiveness and robustness of the new scheme.

1. INTRODUCTION

We consider the initial/boundary value problem for the Schrödinger-Poisson system of finding the *wavefunction* $u : \Omega \times (0, T) \rightarrow \mathbb{C}$ and the *potential* $v : \Omega \times (0, T) \rightarrow \mathbb{R}$ such that

$$(1.1) \quad \begin{cases} u_t - \frac{i\varepsilon}{2\alpha^2} \Delta u + \frac{i}{\varepsilon} v u = 0, & \text{in } \Omega \times (0, T), \\ \Delta v = \frac{\beta}{\alpha} |u|^2, & \text{in } \Omega \times (0, T), \\ u(\mathbf{x}, 0) = u_0(\mathbf{x}), & \text{in } \Omega. \end{cases}$$

The domain $\Omega \subset \mathbb{R}^d$, $d = 1, 2, 3$, is assumed to be bounded, convex and polygonal. The final time $T \in \mathbb{R}^+$ while the data is assumed to satisfy $\alpha, \varepsilon \in \mathbb{R}^+$, $\beta \in \mathbb{R}$ and $u_0 \in H^1(\Omega)$. System (1.1) describes the evolution of the wavefunction $u(\mathbf{x}, t)$ under the influence of a self-consistent potential $v(\mathbf{x}, t)$. The small parameter ε represents the ratio of the Planck constant to the mass of the particle. In this work, system (1.1) will be augmented with periodic or homogeneous Dirichlet boundary conditions which is the case in many practical applications.

The Schrödinger-Poisson system (1.1) has many applications in semiconductor modelling [19], in plasma physics [9] as well as in astrophysics and cosmology where it can be used as an alternative model to the computationally expensive Vlasov-Poisson system [11], [16], [22], [23]. Formally, it is expected as $\varepsilon \rightarrow 0^+$ that the Schrödinger-Poisson system (1.1) approximates, in some sense, the classical Vlasov-Poisson equations, cf., e.g., [26]. Concerning the existence and uniqueness of solutions to the Schrödinger-Poisson system (1.1), we refer to the works [7], [10] and [13]. In [1], the authors analyze a transient Schrödinger-Poisson system with transparent boundary conditions while in [21] the stationary spherically symmetric case was analyzed. The asymptotic behaviour of solutions to the Schrödinger-Poisson system is studied in [2] via a variational approach.

In the literature, there are several methods available for the numerical approximation of solutions to the Schrödinger-Poisson system (1.1). Usually the Crank-Nicolson, Gaussian beam or time splitting method is used for the temporal integration whilst the finite element, finite difference or spectral method is commonly utilized for the spatial discretization. In [3], the authors conduct an error and stability analysis for an operator splitting finite element discretization of (1.1) whilst an error analysis for the semidiscrete Galerkin finite element scheme is presented in [6]. Utilizing a Crank-Nicolson temporal and finite difference spatial discretization of (1.1), a predictor-corrector scheme is studied

Date: December 23, 2024.

Key words and phrases. Schrödinger-Poisson system, Besse relaxation scheme, Crank-Nicolson method, finite element method.

in [20] and the spherically symmetric case is studied in [12]. In [8], the behaviour of the solution of the Schrödinger-Poisson- $X\alpha$ system is explored through a discretization based on the time splitting spectral method. A time semidiscrete scheme for (1.1) using Strang splitting is studied extensively in [17] and an error analysis is provided. The Gaussian beams method is introduced in [14] for the numerical simulation of (1.1) in the one dimensional case whilst in [25] error estimates are obtained for a Crank-Nicolson in time, compact finite difference in space discretization of (1.1). A numerical method consisting of a backward Euler in time, pseudo-spectral method in space is utilized in [24] to approximate the ground states and the evolution of the Schrödinger-Poisson-Slater system (which also includes (1.1)) wavefunction. A spectral discontinuous Galerkin method in space coupled with a Runge-Kutta scheme in time is used to study solutions of (1.1) in [18].

In this work, we introduce a novel numerical scheme for the discretization of the Schrödinger-Poisson system (1.1). We use the standard continuous finite element method for the spatial discretization and the Crank-Nicolson method for the time stepping mechanism. To handle the non-linearity, we utilize the relaxation scheme introduced by Besse [4] for the nonlinear Schrödinger equation which offers a way of linearizing the nonlinear term in the potential equation (1.1). For the Besse discretization of the nonlinear Schrödinger equation, the authors derived a-posteriori error estimates up to the critical exponent in [15]. The main advantage of the scheme is that we avoid solving a computationally expensive nonlinear system whilst maintaining the second order temporal accuracy of the Crank-Nicolson method. The proposed method conserves the density at the discrete level whilst the discrete energy and momentum are preserved to single precision.

The rest of the paper is organized as follows: In Section 2 we derive the conservation laws of the Schrödinger-Poisson system (1.1) while in Section 3 we introduce our new numerical method and derive discrete variants of the system's conservation laws. Section 4 explains the practical implementation of the numerical scheme. In Section 5, we present numerical experiments which verify the accuracy of the method and apply our numerical method to a practical example from cosmology. Finally, we draw conclusions in Section 6.

2. CONSERVATION LAWS

Any solution of the Schrödinger-Poisson system (1.1) satisfies a number of different conservation laws which we'll derive in this section. In order to do this, we need to introduce the *mass density* $\mathcal{D}(t)$, the *energy* $\mathcal{E}(t)$ and the *linear momentum* $\mathcal{M}(t)$, which are defined as follows:

$$(2.1) \quad \mathcal{D}(t) := \|u(t)\|^2,$$

$$(2.2) \quad \mathcal{E}(t) := \frac{\varepsilon^2}{\alpha^2} \|\nabla u(t)\|^2 - \frac{\alpha}{\beta} \|\nabla v(t)\|^2 = \frac{\varepsilon^2}{\alpha^2} \|\nabla u(t)\|^2 + \int_{\Omega} v(t) |u(t)|^2 dx,$$

$$(2.3) \quad \mathcal{M}(t) := -\mathcal{I}m \left(\varepsilon \int_{\Omega} u \nabla \bar{u} dx \right),$$

where $\|\cdot\|$ denotes the L^2 -norm over Ω . With this notation at hand, we are now ready to introduce the conservation laws.

Lemma 2.1. *If (u, v) is a solution of (1.1) then it satisfies the following conservations laws*

$$(2.4) \quad \mathcal{D}(t) = \mathcal{D}(0), \quad \text{Conservation of Mass,}$$

$$(2.5) \quad \mathcal{E}(t) = \mathcal{E}(0), \quad \text{Conservation of Energy,}$$

$$(2.6) \quad \mathcal{M}(t) = \mathcal{M}(0), \quad \text{Conservation of Momentum.}$$

Proof. We begin the proof by deriving conservation of mass. To obtain this, we multiply the Schrödinger equation by \bar{u} and integrate over Ω yielding

$$(2.7) \quad \int_{\Omega} \bar{u} u_t dx + \frac{i\varepsilon}{2\alpha^2} \|\nabla u\|^2 + \frac{i}{\varepsilon} \int_{\Omega} v |u|^2 dx = 0.$$

Taking real parts immediately implies that

$$(2.8) \quad \frac{d\mathcal{D}}{dt} = 0.$$

Hence, upon integration over $(0, t)$, we obtain the equation for conservation of mass:

$$(2.9) \quad \mathcal{D}(t) = \mathcal{D}(0).$$

To derive conservation of energy, we begin by differentiating the potential equation with respect to t yielding

$$(2.10) \quad \Delta \mathbf{v}_t = \frac{\partial}{\partial t} \left(\frac{\beta}{\alpha} |u|^2 \right) = \frac{2\beta}{\alpha} \mathcal{R}e(u \bar{u}_t).$$

Multiplying this by \mathbf{v} and integrating over Ω we get

$$(2.11) \quad -\frac{1}{2} \frac{d}{dt} \|\nabla \mathbf{v}\|^2 = \int_{\Omega} \mathbf{v} \Delta \mathbf{v}_t \, dx = \frac{2\beta}{\alpha} \int_{\Omega} \mathbf{v} \mathcal{R}e(u \bar{u}_t) \, dx.$$

If we instead go to the Schrödinger equation, multiply it by \bar{u}_t and integrate over Ω we obtain

$$(2.12) \quad \int_{\Omega} u_t \bar{u}_t \, dx - \frac{i\varepsilon}{2\alpha^2} \int_{\Omega} \bar{u}_t \Delta u \, dx + \frac{i}{\varepsilon} \int_{\Omega} \mathbf{v} u \bar{u}_t \, dx = 0,$$

or equivalently,

$$(2.13) \quad \|u_t\|^2 + \frac{i\varepsilon}{2\alpha^2} \int_{\Omega} \nabla u \cdot \nabla \bar{u}_t \, dx + \frac{i}{\varepsilon} \int_{\Omega} \mathbf{v} u \bar{u}_t \, dx = 0.$$

Taking imaginary parts yields

$$(2.14) \quad \frac{\varepsilon^2}{4\alpha^2} \frac{d}{dt} \|\nabla u\|^2 + \int_{\Omega} \mathbf{v} \mathcal{R}e(u \bar{u}_t) \, dx = 0.$$

We now substitute in (2.11) to get

$$(2.15) \quad \frac{d\mathcal{E}}{dt} = \frac{d}{dt} \left(\frac{\varepsilon^2}{\alpha^2} \|\nabla u\|^2 - \frac{\alpha}{\beta} \|\nabla \mathbf{v}\|^2 \right) = 0.$$

To obtain the second characterisation of the energy, we multiply the potential equation by \mathbf{v} and integrate over Ω yielding

$$(2.16) \quad \|\nabla \mathbf{v}\|^2 = - \int_{\Omega} \mathbf{v} \Delta \mathbf{v} \, dx = - \frac{\beta}{\alpha} \int_{\Omega} \mathbf{v} |u|^2 \, dx.$$

We then substitute this into (2.15) giving

$$(2.17) \quad \frac{d\mathcal{E}}{dt} = \frac{d}{dt} \left(\frac{\varepsilon^2}{\alpha^2} \|\nabla u\|^2 + \int_{\Omega} \mathbf{v} |u|^2 \, dx \right) = 0.$$

Integrating (2.15) and (2.17) over $(0, t)$ yields the conservation of energy equation:

$$(2.18) \quad \mathcal{E}(t) = \mathcal{E}(0).$$

To show conservation of momentum, we first note via the product rule that we have

$$(2.19) \quad \frac{d\mathcal{M}}{dt} = -\mathcal{I}m \left(\varepsilon \int_{\Omega} \{u_t \nabla \bar{u} + u \nabla \bar{u}_t\} \, dx \right).$$

To evaluate the first term in (2.19), we multiply the Schrödinger equation by $\nabla \bar{u}$ and integrate over Ω to obtain

$$(2.20) \quad \int_{\Omega} u_t \nabla \bar{u} \, dx = \frac{i\varepsilon}{2\alpha^2} \int_{\Omega} \Delta u \nabla \bar{u} \, dx - \frac{i}{\varepsilon} \int_{\Omega} \mathbf{v} u \nabla \bar{u} \, dx.$$

For the second part of (2.19), we conjugate the Schrödinger equation, take its gradient, multiply by u and then integrate over Ω to obtain

$$(2.21) \quad \int_{\Omega} u \nabla \bar{u}_t \, dx = -\frac{i\varepsilon}{2\alpha^2} \int_{\Omega} u \Delta \nabla \bar{u} \, dx + \frac{i}{\varepsilon} \int_{\Omega} u \nabla (\mathbf{v} \bar{u}) \, dx.$$

Integration by parts implies that

$$(2.22) \quad \int_{\Omega} \Delta u \nabla \bar{u} \, dx = \int_{\Omega} u \Delta \nabla \bar{u} \, dx,$$

thus upon substituting (2.20) and (2.21) into (2.19) we obtain

$$(2.23) \quad \begin{aligned} \frac{d\mathcal{M}}{dt} &= -\mathcal{I}m \left(i \int_{\Omega} \{u \nabla(\mathbf{v}\bar{u}) - \mathbf{v}u \nabla\bar{u}\} dx \right) = -\mathcal{I}m \left(i \int_{\Omega} |u|^2 \nabla \mathbf{v} dx \right) \\ &= - \int_{\Omega} |u|^2 \nabla \mathbf{v} dx = -\frac{\alpha}{\beta} \int_{\Omega} \nabla \mathbf{v} \Delta \mathbf{v} dx = \frac{\alpha}{2\beta} \int_{\Omega} \nabla |\nabla \mathbf{v}|^2 dx = 0. \end{aligned}$$

Integrating over $(0, t)$ yields the equation for conservation of momentum (2.6). \square

3. NUMERICAL METHOD

The numerical scheme we propose here is based upon the Crank-Nicolson relaxation method introduced by Besse in [4] for the nonlinear Schrödinger equation. The first stage in the creation of a Besse-style relaxation scheme is to rewrite the system (1.1) via the introduction of an auxiliary variable $\phi = |u|^2$ which takes the place of the nonlinearity. We are thus now searching for a solution (u, \mathbf{v}, ϕ) of the enlarged Schrödinger-Poisson system

$$(3.1) \quad \begin{cases} u_t - \frac{i\varepsilon}{2\alpha^2} \Delta u + \frac{i}{\varepsilon} \mathbf{v}u = 0, & \text{in } \Omega \times (0, T), \\ \Delta \mathbf{v} = \frac{\beta}{\alpha} \phi, & \text{in } \Omega \times (0, T), \\ \phi = |u|^2, & \text{in } \Omega \times (0, T), \\ u(\mathbf{x}, 0) = u_0(\mathbf{x}), & \text{in } \Omega, \end{cases}$$

which is, obviously, equivalent to the original problem (1.1). The numerical scheme that we will introduce in the sequel is based upon this enlarged formulation of the Schrödinger-Poisson system. For the remainder of this section, we assume (1.1)/(3.1) to be augmented with zero Dirichlet boundary conditions for the simplicity of the presentation only as the modification of the numerical method to incorporate periodic boundary conditions is standard and trivial. We begin by first presenting the time semi-discrete scheme before moving on to the presentation of the fully-discrete scheme.

3.1. Time semi-discrete scheme. We begin by introducing a sequence of $N + 1$ *time nodes* $0 =: t_0 < \dots < t_n < \dots < t_N := T$ which induce a partition of $(0, T)$ into N open time intervals $I_n := (t_{n-1}, t_n)$, $n = 1, \dots, N$. The length of the time interval I_n is called the *time step length* and is given by $k_n := |I_n| = t_n - t_{n-1}$. With this notation, our time semi-discrete Besse-type relaxation scheme for (1.1) based on (3.1) is defined as follows: On the interval I_n , we seek approximations $(U^n, V^{n-1/2}, \Phi^{n-1/2}) \in H_0^1(\Omega)$ to $(u(t_n), \mathbf{v}(t_{n-1/2}), \phi(t_{n-1/2})) \in H_0^1(\Omega)$, $1 \leq n \leq N$, such that

$$(3.2) \quad \begin{cases} \bar{\partial} U^n - \frac{i\varepsilon}{2\alpha^2} \Delta U^{n-1/2} + \frac{i}{\varepsilon} V^{n-1/2} U^{n-1/2} = 0, \\ \Delta V^{n-1/2} = \frac{\beta}{\alpha} \Phi^{n-1/2}, \\ \frac{k_{n-1}}{k_{n-1} + k_n} \Phi^{n-1/2} = |U^{n-1}|^2 - \frac{k_n}{k_{n-1} + k_n} \Phi^{n-3/2}, \end{cases}$$

holds with $U^0 = u_0$, $k_0 = k_1$, $\Phi^{-1/2} = |u_0|^2$ and where we used the notation

$$(3.3) \quad t_{n-1/2} := \frac{t_{n-1} + t_n}{2}, \quad U^{n-1/2} := \frac{U^{n-1} + U^n}{2} \quad \text{and} \quad \bar{\partial} U^n := \frac{U^n - U^{n-1}}{k_n}.$$

3.2. Fully-discrete scheme. Let \mathcal{T}_h be a conforming, shape regular partition of Ω consisting of elements K which are either simplices or d -dimensional cubes. We then build real/complex finite element spaces over the mesh \mathcal{T}_h , denoted by $\mathcal{V}_h(\mathcal{T}_h; \mathbb{R})$ and $\mathcal{V}_h(\mathcal{T}_h; \mathbb{C})$, respectively, given by

$$(3.4) \quad \begin{aligned} \mathcal{V}_h(\mathcal{T}_h; \mathbb{R}) &:= \{ \chi \in C(\bar{\Omega}) \cap H_0^1(\Omega) : \forall K \in \mathcal{T}_h, \chi|_K \in \mathbb{P}^r(K) \}, \\ \mathcal{V}_h(\mathcal{T}_h; \mathbb{C}) &:= \{ \chi_R + i\chi_I : \chi_R, \chi_I \in \mathcal{V}_h(\mathcal{T}_h; \mathbb{R}) \}, \end{aligned}$$

where $\mathbb{P}^r(K)$ denotes the space of polynomials on the element K of total degree r if K is a simplex or of degree r in each variable if K is a d -dimensional cube. At each time step n , we assume that

we have some mesh \mathcal{T}_h^n which has been obtained from a previous mesh \mathcal{T}_h^{n-1} via a limited number of refinement and/or coarsening operations. We then associate to each time step n the real and complex finite element spaces $\mathcal{V}_h^n(\mathbb{R}) := \mathcal{V}_h(\mathcal{T}_h^n; \mathbb{R})$ and $\mathcal{V}_h^n(\mathbb{C}) := \mathcal{V}_h(\mathcal{T}_h^n; \mathbb{C})$ over the mesh \mathcal{T}_h^n .

To characterize the fully-discrete scheme on (possibly) variable finite element spaces, we need to introduce two operators; namely, the L^2 -projection operator $\mathcal{P}_h^n : L^2(\Omega) \rightarrow \mathcal{V}_h^n(\mathbb{C})$ and the discrete Laplacian operator $-\Delta_h^n : H_0^1(\Omega) \rightarrow \mathcal{V}_h^n(\mathbb{C})$, which are defined implicitly as the solution of the following variational problems

$$(3.5) \quad v \mapsto \mathcal{P}_h^n v, \quad \langle \mathcal{P}_h^n v, \chi^n \rangle = \langle v, \chi^n \rangle, \quad \forall \chi^n \in \mathcal{V}_h^n(\mathbb{R}),$$

$$(3.6) \quad v \mapsto -\Delta_h^n v, \quad \langle -\Delta_h^n v, \chi^n \rangle = \langle \nabla v, \nabla \chi^n \rangle, \quad \forall \chi^n \in \mathcal{V}_h^n(\mathbb{R}),$$

where $\langle \cdot, \cdot \rangle$ denotes the L^2 -inner product over Ω . Note that although the L^2 -projection/discrete Laplacian may be complex in the above definitions, the test functions always lie in the real finite element space $\mathcal{V}_h^n(\mathbb{R})$. We are now ready to introduce the fully-discrete Besse-style relaxation scheme for (1.1) based on (3.1) which is given as follows: We seek approximations $(U_h^n, V_h^{n-1/2}, \Phi_h^{n-1/2}) \in \mathcal{V}_h^n(\mathbb{C}) \times \mathcal{V}_h^n(\mathbb{R}) \times \mathcal{V}_h^n(\mathbb{R})$ to $(u(\cdot, t_n), v(\cdot, t_{n-1/2}), \phi(\cdot, t_{n-1/2})) \in H_0^1(\Omega)$, $1 \leq n \leq N$, such that

$$(3.7) \quad \begin{cases} \mathcal{P}_h^n \left[\bar{\partial} U_h^n - \frac{i\varepsilon}{4\alpha^2} (\Delta_h^{n-1} U_h^{n-1} + \Delta_h^n U_h^n) + \frac{i}{\varepsilon} V_h^{n-1/2} U_h^{n-1/2} \right] = 0, \\ \Delta_h^n V_h^{n-1/2} = \frac{\beta}{\alpha} \Phi_h^{n-1/2}, \\ \frac{k_{n-1}}{k_{n-1} + k_n} \Phi_h^{n-1/2} = \mathcal{P}_h^n \left[|U_h^{n-1}|^2 - \frac{k_n}{k_{n-1} + k_n} \Phi_h^{n-3/2} \right], \end{cases}$$

where $U_h^0 = \mathcal{P}_h^0 u_0$, $k_0 = k_1$ and $\Phi_h^{-1/2} = |u_0|^2$. If no mesh change occurs on the time step n , i.e., $\mathcal{T}_h^n = \mathcal{T}_h^{n-1}$ then the fully-discrete Besse-style relaxation scheme (3.7) can be simplified to

$$(3.8) \quad \begin{cases} \bar{\partial} U_h^n - \frac{i\varepsilon}{2\alpha^2} \Delta_h^n U_h^{n-1/2} + \frac{i}{\varepsilon} \mathcal{P}_h^n (V_h^{n-1/2} U_h^{n-1/2}) = 0, \\ \Delta_h^n V_h^{n-1/2} = \frac{\beta}{\alpha} \Phi_h^{n-1/2}, \\ \frac{k_{n-1}}{k_{n-1} + k_n} \Phi_h^{n-1/2} = \mathcal{P}_h^n |U_h^{n-1}|^2 - \frac{k_n}{k_{n-1} + k_n} \Phi_h^{n-3/2}. \end{cases}$$

We now look into whether the numerical scheme (3.8) satisfies discrete versions of the system's conservation laws (Lemma 2.1).

The *discrete mass density* is the discrete equivalent of the mass density (2.1) and is given by

$$(3.9) \quad \mathcal{D}_h^n := \|U_h^n\|^2.$$

The discrete mass density satisfies an exact equivalent of the conservation of mass law which is the focus of the following lemma.

Lemma 3.1. *If no mesh change occurs on the time step n , i.e., $\mathcal{T}_h^n = \mathcal{T}_h^{n-1}$ then the solution of the fully-discrete Besse-style relaxation scheme (3.8) satisfies*

$$\mathcal{D}_h^n = \mathcal{D}_h^{n-1}.$$

If no mesh change occurs at all, i.e., $\mathcal{T}_h^n = \dots = \mathcal{T}_h^0$ then

$$\mathcal{D}_h^n = \mathcal{D}_h^0.$$

Proof. We multiply the discrete Schrödinger equation in (3.8) by $\bar{U}_h^{n-1/2}$, i.e, the complex conjugate of $U_h^{n-1/2}$ and integrate over Ω to obtain

$$(3.10) \quad \int_{\Omega} \bar{U}_h^{n-1/2} \bar{\partial} U_h^n \, dx + \frac{i\varepsilon}{2\alpha^2} \|\nabla U_h^{n-1/2}\|^2 + \frac{i}{\varepsilon} \int_{\Omega} V_h^{n-1/2} |U_h^{n-1/2}|^2 \, dx = 0.$$

The last two terms are purely imaginary so taking real parts and expanding yields

$$(3.11) \quad \mathcal{D}_h^n - \mathcal{D}_h^{n-1} + \int_{\Omega} \operatorname{Re}(U_h^n \bar{U}_h^{n-1} - U_h^{n-1} \bar{U}_h^n) \, dx = 0.$$

The last integral vanishes and so we are left with

$$(3.12) \quad \mathcal{D}_h^n = \mathcal{D}_h^{n-1},$$

as claimed. \square

In contrast to mass conservation, the discrete solution of (3.8) does not satisfy an exact analogue of the conservation of energy law (2.5). When trying to decide how to define the discrete energy, we recall that there are two equivalent formulations of the continuous energy (2.2) which are unlikely to be the same when discretized. Unfortunately, we observed during numerical experiments that discretizing either of the two continuous definitions results in the corresponding error oscillating wildly between time steps whereas we would prefer for it to be a more stable quantity. As the two definitions of the continuous energy (2.2) are equal, any linear combination of the two is also a conservation law thus we can also discretize this linear combination. It transpires that defining the *discrete energy* by

$$(3.13) \quad \mathcal{E}_h^n := \frac{\varepsilon^2}{\alpha^2} \|\nabla U_h^n\|^2 + \frac{\alpha}{\beta} \|\nabla V_h^n\|^2 + 2 \int_{\Omega} V_h^n |U_h^n|^2 dx,$$

results in a stable quantity which does not oscillate between time steps. As already mentioned, the discrete energy does not satisfy an exact analogue of the conservation of energy law (2.5). The aim of the next lemma is to quantify the error involved in the discrete energy.

Lemma 3.2. *If no mesh change occurs on the time step n then the solution of the fully-discrete Besse-style relaxation scheme (3.8) satisfies*

$$\mathcal{E}_h^n = \mathcal{E}_h^{n-1} + \frac{\alpha}{\beta} (\|\nabla V_h^n\|^2 - \|\nabla V_h^{n-1}\|^2) + 2 \int_{\Omega} (V_h^n - V_h^{n-1/2}) |U_h^n|^2 dx - 2 \int_{\Omega} (V_h^{n-1} - V_h^{n-1/2}) |U_h^{n-1}|^2 dx.$$

Proof. Multiplying the discrete Schrödinger equation (3.8) by $\overline{\partial U_h^n}$ and integrating over Ω we obtain

$$(3.14) \quad \|\overline{\partial U_h^n}\|^2 + \frac{i\varepsilon}{2\alpha^2} \int_{\Omega} \nabla U_h^{n-1/2} \cdot \nabla \overline{\partial U_h^n} dx + \frac{i}{\varepsilon} \int_{\Omega} V_h^{n-1/2} U_h^{n-1/2} \overline{\partial U_h^n} dx = 0.$$

Taking imaginary parts yields

$$(3.15) \quad \frac{\varepsilon}{4\alpha^2 k_n} (\|\nabla U_h^n\|^2 - \|\nabla U_h^{n-1}\|^2) + \frac{1}{2\varepsilon k_n} \int_{\Omega} V_h^{n-1/2} (|U_h^n|^2 - |U_h^{n-1}|^2) dx = 0.$$

Or equivalently

$$(3.16) \quad \frac{\varepsilon^2 k_n}{\alpha^2} \overline{\partial} \|\nabla U_h^n\|^2 + 2k_n \int_{\Omega} V_h^{n-1/2} \overline{\partial} |U_h^n|^2 dx = 0.$$

The result then follows from the definition of the discrete energy \mathcal{E}_h^n . \square

Remark 3.1. *Formally, the right-hand side in Lemma 3.2 is only order one locally and thus constant globally; nevertheless, we observe numerically in the sequel that the energy error is $\mathcal{O}(k^3)$ locally and $\mathcal{O}(k^2)$ globally where $k := \max_{1 \leq n \leq N} k_n$ is the maximum time step length. We were unable to prove this but it should be possible through Lemma 3.2 and by further invoking (3.8).*

The discrete version of the momentum operator is given by

$$(3.17) \quad \mathcal{M}_h^n := -\mathcal{I}m \left(\varepsilon \int_{\Omega} U_h^n \nabla \overline{U_h^n} dx \right).$$

As with the discrete energy, the scheme (3.8) does not preserve the discrete momentum. For the discrete momentum, we have the following lemma which characterizes the error incurred.

Lemma 3.3. *If no mesh change occurs on the time step n then the solution of the fully-discrete Besse-style relaxation scheme (3.8) satisfies*

$$\begin{aligned} \mathcal{M}_h^n = \mathcal{M}_h^{n-1} - k_n \left[\int_{\Omega} |U_h^{n-1/2}|^2 \nabla V_h^{n-1/2} dx + \frac{\varepsilon^2}{\alpha^2} \mathcal{R}e \left(\int_{\Omega} \nabla U_h^{n-1/2} \Delta_h^n \overline{U_h^{n-1/2}} dx \right) \right. \\ \left. - 2 \mathcal{R}e \left(\int_{\Omega} (\mathcal{P}_h^n - I) (V_h^{n-1/2} U_h^{n-1/2}) \nabla \overline{U_h^{n-1/2}} dx \right) \right]. \end{aligned}$$

Proof. The discrete product rule

$$(3.18) \quad \bar{\partial}(V_h^n W_h^n) = V_h^{n-1/2} \bar{\partial} W_h^n + W_h^{n-1/2} \bar{\partial} V_h^n,$$

implies that

$$(3.19) \quad \bar{\partial} \mathcal{M}_h^n = -\mathcal{I}m \left(\varepsilon \int_{\Omega} \{ U_h^{n-1/2} \bar{\partial} \nabla \bar{U}_h^n + \nabla \bar{U}_h^{n-1/2} \bar{\partial} U_h^n \} dx \right).$$

For the first term, we conjugate the strong form of the numerical scheme (3.8), take its gradient, multiply by $U_h^{n-1/2}$ and integrate over Ω to obtain

$$(3.20) \quad \int_{\Omega} U_h^{n-1/2} \bar{\partial} \nabla \bar{U}_h^n dx = -\frac{i\varepsilon}{2\alpha^2} \int_{\Omega} U_h^{n-1/2} \nabla \Delta_h^n \bar{U}_h^{n-1/2} dx + \frac{i}{\varepsilon} \int_{\Omega} U_h^{n-1/2} \nabla \mathcal{P}_h^n (V_h^{n-1/2} \bar{U}_h^{n-1/2}) dx.$$

For the second term, we multiply the strong form of the numerical scheme (3.8) by $\nabla \bar{U}_h^{n-1/2}$ and integrate over Ω to obtain

$$(3.21) \quad \int_{\Omega} \nabla \bar{U}_h^{n-1/2} \bar{\partial} U_h^n dx = \frac{i\varepsilon}{2\alpha^2} \int_{\Omega} \nabla \bar{U}_h^{n-1/2} \Delta_h^n U_h^{n-1/2} dx - \frac{i}{\varepsilon} \int_{\Omega} \nabla \bar{U}_h^{n-1/2} \mathcal{P}_h^n (V_h^{n-1/2} U_h^{n-1/2}) dx.$$

Substituting (3.20) and (3.21) into (3.19) yields

$$(3.22) \quad \begin{aligned} \bar{\partial} \mathcal{M}_h^n &= \mathcal{I}m \left(\frac{i\varepsilon^2}{2\alpha^2} \int_{\Omega} \{ U_h^{n-1/2} \nabla \Delta_h^n \bar{U}_h^{n-1/2} - \nabla \bar{U}_h^{n-1/2} \Delta_h^n U_h^{n-1/2} \} dx \right) \\ &\quad + \mathcal{I}m \left(i \int_{\Omega} \{ \mathcal{P}_h^n (V_h^{n-1/2} U_h^{n-1/2}) \nabla \bar{U}_h^{n-1/2} - U_h^{n-1/2} \nabla \mathcal{P}_h^n (V_h^{n-1/2} \bar{U}_h^{n-1/2}) \} dx \right). \end{aligned}$$

Continuing the proof along the lines of the proof of conservation of momentum in Lemma 2.1 we quickly run into problems because $\nabla U_h^n \notin \mathcal{V}_h^n(\mathbb{C})$ meaning we cannot substitute for the operators Δ_h^n and \mathcal{P}_h^n in (3.22).

The first term in (3.22) can be written more compactly as follows

$$(3.23) \quad \begin{aligned} &\mathcal{I}m \left(\frac{i\varepsilon^2}{2\alpha^2} \int_{\Omega} \{ U_h^{n-1/2} \nabla \Delta_h^n \bar{U}_h^{n-1/2} - \nabla \bar{U}_h^{n-1/2} \Delta_h^n U_h^{n-1/2} \} dx \right) \\ &= \mathcal{I}m \left(\frac{i\varepsilon^2}{2\alpha^2} \int_{\Omega} \{ \nabla (U_h^{n-1/2} \Delta_h^n \bar{U}_h^{n-1/2}) - \nabla U_h^{n-1/2} \Delta_h^n \bar{U}_h^{n-1/2} - \nabla \bar{U}_h^{n-1/2} \Delta_h^n U_h^{n-1/2} \} dx \right) \\ &= -\mathcal{I}m \left(\frac{i\varepsilon^2}{\alpha^2} \mathcal{R}e \left(\int_{\Omega} \nabla U_h^{n-1/2} \Delta_h^n \bar{U}_h^{n-1/2} dx \right) \right) = -\frac{\varepsilon^2}{\alpha^2} \mathcal{R}e \left(\int_{\Omega} \nabla U_h^{n-1/2} \Delta_h^n \bar{U}_h^{n-1/2} dx \right), \end{aligned}$$

but we were unable to manipulate this term further in order to obtain a more meaningful expression. By contrast, the second term in (3.22) can be rewritten more meaningfully by adding and subtracting the identity operator, viz.,

$$(3.24) \quad \begin{aligned} &i \int_{\Omega} \{ \mathcal{P}_h^n (V_h^{n-1/2} U_h^{n-1/2}) \nabla \bar{U}_h^{n-1/2} - U_h^{n-1/2} \nabla \mathcal{P}_h^n (V_h^{n-1/2} \bar{U}_h^{n-1/2}) \} dx \\ &= i \int_{\Omega} \{ (\mathcal{P}_h^n - I)(V_h^{n-1/2} U_h^{n-1/2}) \nabla \bar{U}_h^{n-1/2} - U_h^{n-1/2} \nabla (\mathcal{P}_h^n - I)(V_h^{n-1/2} \bar{U}_h^{n-1/2}) \} dx \\ &\quad + i \int_{\Omega} \{ V_h^{n-1/2} U_h^{n-1/2} \nabla \bar{U}_h^{n-1/2} - U_h^{n-1/2} \nabla (V_h^{n-1/2} \bar{U}_h^{n-1/2}) \} dx. \end{aligned}$$

We then follow the arguments from (3.23) and Lemma 2.1 in order to determine that

$$(3.25) \quad \begin{aligned} &\mathcal{I}m \left(i \int_{\Omega} \{ \mathcal{P}_h^n (V_h^{n-1/2} U_h^{n-1/2}) \nabla \bar{U}_h^{n-1/2} - U_h^{n-1/2} \nabla \mathcal{P}_h^n (V_h^{n-1/2} \bar{U}_h^{n-1/2}) \} dx \right) \\ &= 2 \mathcal{R}e \left(\int_{\Omega} (\mathcal{P}_h^n - I)(V_h^{n-1/2} U_h^{n-1/2}) \nabla \bar{U}_h^{n-1/2} dx \right) - \int_{\Omega} |U_h^{n-1/2}|^2 \nabla V_h^{n-1/2} dx. \end{aligned}$$

Substituting (3.23) and (3.25) into (3.22) completes the proof. \square

4. IMPLEMENTATION

In this section, we discuss the practicalities of implementing the Besse-style relaxation scheme (3.7) for the numerical solution of the Schrödinger-Poisson system (1.1).

4.1. Solving for the nonlinearity. Solving for the nonlinearity is a standard finite element problem, i.e., we are seeking a vector of coefficients $\widehat{\Phi}_h^{n-1/2}$ for $\Phi_h^{n-1/2}$ such that

$$\Phi_h^{n-1/2} = \sum_{j=1}^{\mathcal{N}_n} \widehat{\Phi}_{h,j}^{n-1/2} \varphi_j^n,$$

where φ_j^n , $j = 1, \dots, \mathcal{N}_n = \dim(\mathcal{V}_h^n(\mathbb{R}))$ are (real) finite element basis functions. From (3.7), we see that the vector of coefficients $\widehat{\Phi}_h^{n-1/2}$ must satisfy

$$\frac{k_{n-1}}{k_{n-1} + k_n} M \widehat{\Phi}_h^{n-1/2} = \left(\left\langle |U_h^{n-1}|^2 - \frac{k_n}{k_{n-1} + k_n} \Phi_h^{n-3/2}, \varphi_j^n \right\rangle_{j=1, \dots, \mathcal{N}_n} \right),$$

where M is the *mass matrix* given by

$$M_{ij} = \int_{\Omega} \varphi_i^n \varphi_j^n \, dx.$$

For the first interval, we need to take particular care to ensure that $\Phi_h^{1/2}$ is order two, otherwise, the scheme degrades and becomes order one. In particular, it is not sufficient to calculate $\Phi_h^{1/2}$ as proposed in (3.7) with $\Phi_h^{-1/2} = |u_0|^2$ – we need a better approximation to $\Phi_h^{1/2}$. Doubtless, there are many ways to achieve this. In this paper, we propose computing an initial approximation $\Phi_{h,\text{old}}^{1/2}$ to the nonlinearity as originally given in (3.7). $\Phi_{h,\text{old}}^{1/2}$ is then used in the numerical scheme (3.7) to calculate initial approximations for the potential and wavefunction which we denote by $\widetilde{V}_h^{1/2}$ and \widetilde{U}_h^1 , respectively. The initial approximation to the wavefunction, \widetilde{U}_h^1 , is then used to update the estimate for the nonlinearity on the first time step. In particular, the coefficients $\widehat{\Phi}_h^{1/2}$ are chosen to satisfy

$$M \widehat{\Phi}_h^{1/2} = \left(\left\langle \frac{1}{2} |\widetilde{U}_h^1|^2 + \frac{1}{2} \Phi_{h,\text{old}}^{1/2}, \varphi_j^1 \right\rangle_{j=1, \dots, \mathcal{N}_1} \right).$$

Computing $\Phi_h^{1/2}$ in this way ensures that the nonlinear part of the scheme is order two on the first time interval and, thus, order two on any time step n . Interestingly, it was observed for at least one numerical example that U_h remains order two even when $\Phi_h^{1/2} = \Phi_{h,\text{old}}^{1/2}$, however, V_h was only order one under this choice.

4.2. Solving for the potential. Solving for the potential is also fairly routine; if we introduce the vector of coefficients $\widehat{V}_h^{n-1/2}$ such that

$$V_h^{n-1/2} = \sum_{j=1}^{\mathcal{N}_n} \widehat{V}_{h,j}^{n-1/2} \varphi_j^n,$$

then (3.7) implies that $\widehat{V}_h^{n-1/2}$ must satisfy

$$L \widehat{V}_h^{n-1/2} = \left(\frac{-\beta}{\alpha} \langle \Phi_h^{n-1/2}, \varphi_j^n \rangle_{j=1, \dots, \mathcal{N}_n} \right),$$

where L is the *Laplace matrix* given by

$$L_{ij} = \int_{\Omega} \nabla \varphi_i^n \cdot \nabla \varphi_j^n \, dx.$$

For V_h^0 , the coefficients \widehat{V}_h^0 are chosen to satisfy the matrix-vector system

$$L \widehat{V}_h^0 = \left(\frac{-\beta}{\alpha} \langle \Phi_{h,\text{old}}^{1/2}, \varphi_j^0 \rangle_{j=1, \dots, \mathcal{N}_0} \right).$$

An important question now arises: how do we extend these nodal values so that $V_h(t)$ is of optimal order in time? On the first interval, it is relatively clear that we should linearly interpolate through V_h^0 and $V_h^{1/2}$ to obtain V_h^1 , i.e., we set $V_h^1 = 2V_h^{1/2} - V_h^0$. We can then define

$$V_h(t) := \left(\frac{t - t_0}{k_1} \right) V_h^1 + \left(\frac{t_1 - t}{k_1} \right) V_h^0, \quad t \in \bar{I}_1.$$

It is tempting to continue to iterate this procedure in order to compute the remaining nodal values, however, after the first interval, the value V_h^n is an *interpolated quantity*. Attempting to calculate V_h^n by interpolating through V_h^{n-1} (an interpolated point) and $V_h^{n-1/2}$ (a calculated point) is therefore an unstable procedure which oscillates out of control. To avoid this, we instead calculate V_h^n by linearly interpolating through the computed values $V_h^{n-1/2}$ and $V_h^{n-3/2}$; a simple calculation yields

$$V_h^n = V_h^{n-1/2} + \frac{k_n}{k_{n-1} + k_n} (V_h^{n-1/2} - V_h^{n-3/2}).$$

A variety of options now exist as to how we can define $V_h(t)$ on \bar{I}_n using the three nodal values V_h^{n-1} , $V_h^{n-1/2}$ and V_h^n . We opt for the “standard” approach of defining $V_h(t)$ to be the linear interpolant through the extremal nodes, i.e., we set

$$V_h(t) := \left(\frac{t_n - t}{k_n} \right) V_h^{n-1} + \left(\frac{t - t_{n-1}}{k_n} \right) V_h^n, \quad t \in \bar{I}_n.$$

We remark, however, that this approach does have a drawback: in general, $V_h(t_{n-1/2}) \neq V_h^{n-1/2}$ (although this does not affect the order of V_h).

4.3. Solving for the wavefunction. In the case of the wavefunction, we are seeking a vector of real coefficients $\hat{U}_{h,R}^n$ and a vector of imaginary coefficients $\hat{U}_{h,I}^n$ such that

$$U_h^n = U_{h,R}^n + iU_{h,I}^n = \sum_{j=1}^{\mathcal{N}_n} (\hat{U}_{h,R,j}^n + i\hat{U}_{h,I,j}^n) \varphi_j^n.$$

Here, as before, φ_j^n , $j = 1, \dots, \mathcal{N}_n = \dim(\mathcal{V}_h^n(\mathbb{R}))$ are *real* finite element basis functions which form a basis for $\mathcal{V}_h^n(\mathbb{R})$. Then (3.7) implies that the coefficient vectors must satisfy the block matrix-vector system

$$(4.1) \quad \begin{pmatrix} M & -\frac{\varepsilon k_n}{4\alpha^2} L - \frac{k_n}{2\varepsilon} P \\ \frac{\varepsilon k_n}{4\alpha^2} L + \frac{k_n}{2\varepsilon} P & M \end{pmatrix} \begin{pmatrix} \hat{U}_{h,R}^n \\ \hat{U}_{h,I}^n \end{pmatrix} = \begin{pmatrix} \langle U_{h,R}^{n-1} - \frac{\varepsilon k_n}{4\alpha^2} \Delta_h^{n-1} U_{h,I}^{n-1} + \frac{k_n}{2\varepsilon} V_h^{n-1/2} U_{h,I}^{n-1}, \varphi_j^n \rangle_{j=1, \dots, \mathcal{N}_n} \\ \langle U_{h,I}^{n-1} + \frac{\varepsilon k_n}{4\alpha^2} \Delta_h^{n-1} U_{h,R}^{n-1} - \frac{k_n}{2\varepsilon} V_h^{n-1/2} U_{h,R}^{n-1}, \varphi_j^n \rangle_{j=1, \dots, \mathcal{N}_n} \end{pmatrix},$$

where Δ_h^{n-1} is the discrete Laplacian operator (see (3.6)) and P , the matrix associated with the potential term, is given by

$$P_{ij} = \int_{\Omega} V_h^{n-1/2} \varphi_i^n \varphi_j^n \, dx.$$

As is standard, we extend the nodal values of the wavefunction to a function $U_h(t)$ on the whole interval via linear interpolation, viz.,

$$U_h(t) := \left(\frac{t_n - t}{k_n} \right) U_h^{n-1} + \left(\frac{t - t_{n-1}}{k_n} \right) U_h^n, \quad t \in \bar{I}_n.$$

As a side, we note that (4.1) can be solved far more efficiently if no mesh change has occurred. Indeed, in this case the system (3.7) can be rewritten to solve for the half point $U_h^{n-1/2}$ (3.8) resulting in the block matrix-vector system

$$\begin{pmatrix} M & -\frac{\varepsilon k_n}{4\alpha^2} L - \frac{k_n}{2\varepsilon} P \\ \frac{\varepsilon k_n}{4\alpha^2} L + \frac{k_n}{2\varepsilon} P & M \end{pmatrix} \begin{pmatrix} \hat{U}_{h,R}^{n-1/2} \\ \hat{U}_{h,I}^{n-1/2} \end{pmatrix} = \begin{pmatrix} M & 0 \\ 0 & M \end{pmatrix} \begin{pmatrix} \hat{U}_{h,R}^{n-1} \\ \hat{U}_{h,I}^{n-1} \end{pmatrix}.$$

The nodal value coefficients \widehat{U}_h^n can then be recovered via $\widehat{U}_h^n = 2\widehat{U}_h^{n-1/2} - \widehat{U}_h^{n-1}$.

5. NUMERICAL EXPERIMENTS

We perform two sets of numerical experiments. The purpose of the first two numerical experiments is to apply the new numerical method (3.7) to some simple problems in order to confirm basic properties of the method such as the rate of convergence and to quantify the discrete conservation law errors. The second set of numerical experiments involves applying (3.7) to an example emanating from the field of cosmology (“sine wave collapse”) where the Schrödinger-Poisson system (1.1) is used as a lower dimensional model for the more complex Vlasov-Poisson system [16]. The numerical results reported in this section take place in two spatial dimensions and utilize a C++ code based on the `deal.II` finite element library [5].

5.1. Experimental order of convergence. To verify the experimental order of convergence of the numerical method, we apply the classical method of manufactured solutions, i.e., we choose a wavefunction $u(\mathbf{x}, t) : \Omega \times [0, T] \rightarrow \mathbb{C}$ and a potential $v(\mathbf{x}, t) : \Omega \times [0, T] \rightarrow \mathbb{R}$ such that (1.1) is satisfied (with the inclusion of appropriate right-hand sides). Here, we set $\Omega = (-1, 1)^2 \subset \mathbb{R}^2$ and consider uniform partitions \mathcal{T}_h of Ω consisting of squares with sides of length h . For simplicity, we set the PDE coefficients to $\alpha = \beta = \varepsilon = 1$ with the final time given by $T = 1$ and the time interval $(0, T)$ subdivided into uniform intervals of time step length $k = T/N > 0$. We choose the right-hand sides such that the exact solution to (1.1) is given by

$$v(x, y, t) = e^{-t} \sin(\pi(x^2 - 1)(y^2 - 1)), \quad u(x, y, t) = (1 + i)v(x, y, t).$$

The errors are then measured in the $L^\infty L^2$ norm and we expect that

$$e(u; h, k) := \max_{0 \leq n \leq N} \|u(\cdot, t_n) - U_h^n\| = \mathcal{O}(k^2 + h^{r+1}), \quad e(v; h, k) := \max_{0 \leq n \leq N} \|v(\cdot, t_n) - V_h^n\| = \mathcal{O}(k^2 + h^{r+1}),$$

where r is the polynomial degree of the spatial finite element space $\mathcal{V}_h(\mathcal{T}_h; \mathbb{R})$.

We begin by taking large number of time steps, $N = 2000$, so that the temporal part of the error is negligible. We then compute the spatial experimental order of convergence by performing two different realizations with the mesh sizes h_1 and h_2 and computing

$$\text{Rate} := \frac{\log(e(\cdot; h_1, k)) - \log(e(\cdot; h_2, k))}{\log(h_1) - \log(h_2)}.$$

In Table 1, the spatial experimental orders of convergence are displayed for $r = 1$ and $r = 2$. The optimal rate of convergence is observed in both cases thus validating the claimed spatial accuracy of our new numerical method (3.7).

TABLE 1. Spatial experimental orders of convergence.

h	$r = 1$				$r = 2$			
	$e(u; k, h)$	Rate	$e(v; k, h)$	Rate	$e(u; k, h)$	Rate	$e(v; k, h)$	Rate
0.250000	2.60203e-1	-	1.36736e-1	-	1.54310e-2	-	8.50485e-3	-
0.125000	6.58945e-2	1.981	3.29791e-2	2.052	2.19359e-3	2.814	1.31987e-3	2.688
0.062500	1.68103e-2	1.971	8.23356e-3	2.002	2.54266e-4	3.109	1.71600e-4	2.943
0.031250	4.22146e-3	1.994	2.05895e-3	2.000	3.12572e-5	3.024	2.16460e-5	2.987
0.015625	1.05487e-3	2.001	5.14783e-4	2.000	3.85637e-6	3.019	2.71179e-6	2.997

Next, we take a large polynomial degree, $r = 9$, in order to minimize the spatial error over the uniform spatial mesh \mathcal{T}_h of mesh size $h = 0.0625$. We then compute the temporal experimental order of convergence by performing two different realizations with the time step lengths k_1 and k_2 and computing

$$\text{Rate} := \frac{\log(e(\cdot; h, k_1)) - \log(e(\cdot; h, k_2))}{\log(k_1) - \log(k_2)}.$$

TABLE 2. Temporal experimental orders of convergence.

k	$e(u; k, h)$	Rate	$e(v; k, h)$	Rate
0.04	3.72233e-4	-	9.60801e-4	-
0.02	9.49430e-5	1.971	2.51017e-4	1.936
0.01	2.39046e-5	1.990	6.41950e-5	1.967

The results, given in Table 2, confirm that our proposed numerical method (3.7) is order two in time for both the wavefunction u and the potential v .

5.2. Conservation of invariants. In this example, we investigate the behaviour of our numerical scheme (3.7) with respect to the invariant quantities (2.4), (2.5) and (2.6). We again set $\Omega = (-1, 1)^2$ which we discretize with linear finite elements over a uniform grid \mathcal{T}_h consisting of squares with sides of length $h = 0.015625$. The final time is chosen to be $T = 3$ and we use $N = 3000$ time steps giving a time step length of 0.001. The coefficients in (1.1) are set to $\alpha = \beta = 5$ with the exception of ε which is allowed to vary in order to analyze how this affects the errors in the conservation laws. The initial condition is given by

$$u(x, y, 0) = (\sin(x) + i \cos(y))(1 - x^2)^2(1 - y^2)^2.$$

We now compute the conservation law errors given by

$$(5.1) \quad \mathcal{D}_e^n := \left| \|U_h^n\|^2 - \|u_0\|^2 \right|,$$

$$(5.2) \quad \mathcal{E}_e^n := \left| \left(\frac{\varepsilon^2}{\alpha^2} \|\nabla U_h^n\|^2 + \frac{\alpha}{\beta} \|\nabla V_h^n\|^2 + 2 \int_{\Omega} V_h^n |U_h^n|^2 dx \right) - \left(\frac{\varepsilon^2}{\alpha^2} \|\nabla u_0\|^2 + \frac{\alpha}{\beta} \|\nabla v(\cdot, 0)\|^2 + 2 \int_{\Omega} v(\cdot, 0) |u_0|^2 dx \right) \right|,$$

$$(5.3) \quad \mathcal{M}_e^n := \left| \operatorname{Im} \left(\varepsilon \int_{\Omega} U_h^n \nabla \bar{U}_h^n dx \right) - \operatorname{Im} \left(\varepsilon \int_{\Omega} u_0 \nabla \bar{u}_0 dx \right) \right|,$$

which are the differences between the invariants (2.4), (2.5), (2.6) and their discrete counterparts. From Table 3, we observe that the density is conserved up to double precision accuracy for all values of ε as expected. The energy is also conserved up to double precision accuracy while the error in the momentum is single precision for all ε values tested.

TABLE 3. Errors in the conservation laws.

	$\varepsilon = 1$			$\varepsilon = 0.1$			$\varepsilon = 0.01$		
t_n	\mathcal{D}_e^n	\mathcal{E}_e^n	\mathcal{M}_e^n	\mathcal{D}_e^n	\mathcal{E}_e^n	\mathcal{M}_e^n	\mathcal{D}_e^n	\mathcal{E}_e^n	\mathcal{M}_e^n
0	5.44e-15	1.58e-15	1.42e-09	3.77e-15	4.44e-16	1.09e-10	3.66e-15	3.96e-16	1.09e-11
1	4.12e-14	8.82e-12	5.71e-03	1.32e-14	1.95e-12	1.11e-04	3.32e-14	2.02e-12	1.11e-05
2	7.75e-14	2.65e-11	2.67e-02	3.34e-14	8.20e-12	4.44e-04	6.32e-14	8.79e-12	4.58e-05
3	1.31e-13	4.83e-11	5.91e-02	4.42e-14	2.00e-11	9.97e-04	8.99e-14	2.30e-11	1.10e-04

TABLE 4. Convergence of the conservation law errors.

k	\mathcal{E}_e^N	Rate	\mathcal{M}_e^N
0.01000	2.28194e-09	-	1.08815e-04
0.00500	5.74214e-10	1.991	1.09436e-04
0.00250	1.43736e-10	1.998	1.09592e-04
0.00125	3.58843e-11	2.002	1.09631e-04

Next, we test how the conservation law errors behave for $\varepsilon = 0.01$ as we reduce the time step length k . Recall from Section 4 that we expect that $\mathcal{E}_e^N = \mathcal{O}(k^2)$ which is indeed what we observe in Table 4. By contrast, surprisingly, the momentum error \mathcal{M}_e^N does not reduce as either $k \rightarrow 0^+$ or as $h \rightarrow 0^+$ instead remaining more or less constant.

5.3. A cosmological example. One application of the Schrödinger-Poisson system (1.1) comes from the field of cosmology. Indeed, the d -dimensional Schrödinger-Poisson system (1.1) can be used as an approximation to the computationally expensive $2d$ -dimensional Vlasov-Poisson system used to describe collisionless self-gravitating matter [16].

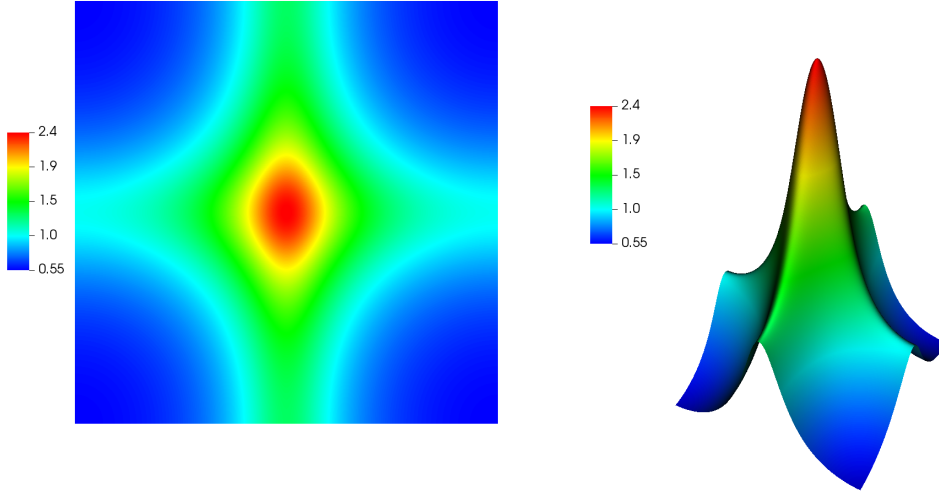


FIGURE 1. The initial density $|u_0|^2$.

For this numerical experiment, we proceed as in [16]. Firstly, the potential equation in (1.1) is modified to account for cosmological boundary conditions, viz.,

$$\Delta \mathbf{v} = \frac{\beta}{\alpha} (|u|^2 - 1).$$

We then make the change of variables $d\alpha = \alpha^{-1/2} dt$ and, to avoid ambiguity, make the notational exchange $\alpha \leftrightarrow \tau$. With these modifications, the system (1.1) now reads as follows

$$(5.4) \quad \begin{cases} u_\tau - \frac{i\varepsilon}{2\tau^{3/2}} \Delta u + \frac{i\tau^{1/2}}{\varepsilon} \mathbf{v}u = 0, & \text{in } \Omega \times (\tau_i, \tau_f), \\ \Delta \mathbf{v} = \frac{\beta}{\tau} (|u|^2 - 1), & \text{in } \Omega \times (\tau_i, \tau_f), \\ u(\mathbf{x}, 0) = u_0(\mathbf{x}), & \text{in } \Omega. \end{cases}$$

This new Schrödinger-Poisson system (5.4) is augmented with periodic boundary conditions for both u and \mathbf{v} and the numerical scheme (3.7) modified appropriately for the new system. We now consider a benchmark case, namely, “sine wave collapse”. We set $\Omega = (-0.5, 0.5)^2$, $\tau_i = 0.01$, $\tau_f = 0.088$, $\beta = 1.5$ and $\varepsilon = 6e-5$. The initial condition is as given in [16] and is displayed in Figure 1.

The domain Ω is discretized with linear finite elements over one of two different uniform grids: a 1024×1024 and a 2048×2048 grid while the time domain (τ_i, τ_f) is discretized using 1560 uniform time steps yielding a time step size of $k = 5e-5$. Results of the numerical simulations are shown in Figure 3. For comparison purposes, we plot the density $|U_h(\tau)|^2$ at three different time instances ($\tau = 0.023, 0.033, 0.088$) all of which are in *excellent* agreement with the plots in [16].

Due to the small value of ε , the wavefunction is highly oscillatory which can be readily seen in the 1024×1024 grid but is much more apparent in the 2048×2048 grid. We thus postprocess

the density by applying a Gaussian filter of width $\sigma = 0.0035$ which eliminates all oscillations of relatively small amplitude – this is shown in Figure 2 at the final time $\tau = \tau_f$ for both grids.

For this example, the density is again conserved up to double precision while the energy (appropriately modified for the new system (5.4)) and momentum are conserved up to 3 and 7 digits of accuracy, respectively.

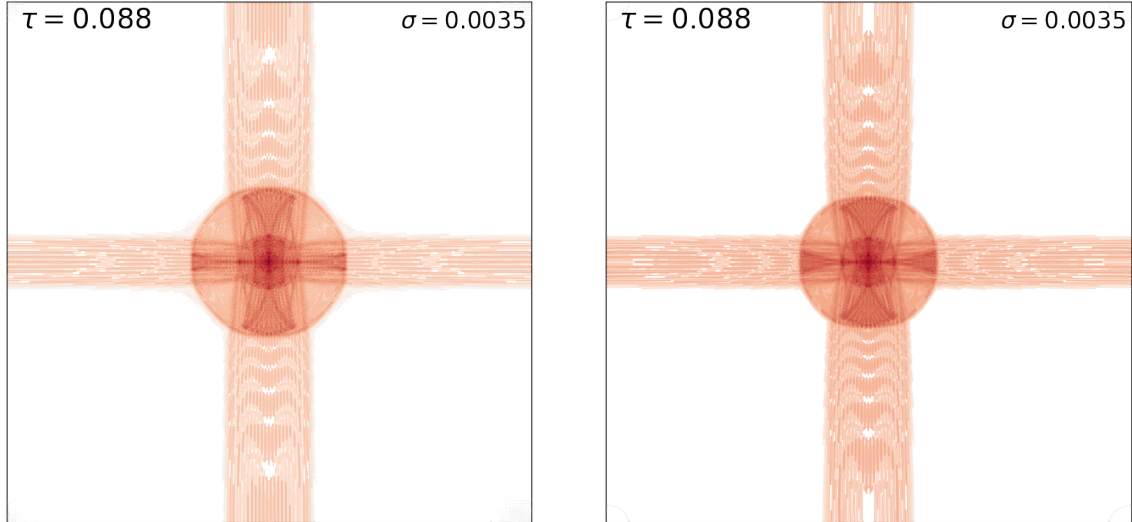


FIGURE 2. The density $|U_h(\tau)|^2$ (logarithmic scale) at $\tau = \tau_f$ with Gaussian filtering of width $\sigma = 0.0035$: 1024×1024 grid (left), 2048×2048 grid (right).

6. CONCLUSIONS

We proposed a new numerical method (3.7) for the numerical solution of the Schrödinger–Poisson system (1.1) which is order two in time and of optimal order in space. The numerical method does not utilize the nonlinearity directly so no nonlinear iteration, i.e., a Newton method, is required making the method fast as well as accurate. The numerical method conserves mass and was observed to conserve energy with an error proportional to the order of the method. In the future, our ultimate goal is to use the scheme (3.7) to efficiently model structure formation in three spatial dimensions.

ACKNOWLEDGEMENTS

The authors would like to express their gratitude to K. Vattis, Prof. C. Skordis and especially Prof. M. Kopp for their valuable help and guidance in setting up the cosmological example reported in Section 5.

REFERENCES

- [1] N.B. Abdallah, F. Méhats and O. Pinaud, *On an open transient Schrödinger–Poisson system*, Mathematical Models and Methods in Applied Sciences (M3AS) 15(5), pp. 667–688, 2005
- [2] E. Arriola and J. Soler, *A variational approach to the Schrödinger–Poisson System: Asymptotic behaviour, breathers, and stability*, Journal of Statistical Physics 103, 1069–1106, 2001.
- [3] W. Auzinger, T. Kassebacher, O. Koch and M. Thalhammer, *Convergence of a Strang splitting finite element discretization for the Schrödinger–Poisson equation*, ESAIM: M2AN 51, 1245–1278, 2017.
- [4] Ch. Besse, *A relaxation scheme for the nonlinear Schrödinger equation*, SIAM J. Numer. Anal. 42, 934–952, 2004.
- [5] W. Bangerth, R. Hartmann and G. Kanschat, **deal.II** – *A general-purpose object-oriented finite element library*, ACM Transactions on Mathematical Software, 33(4), article 24, 2007.

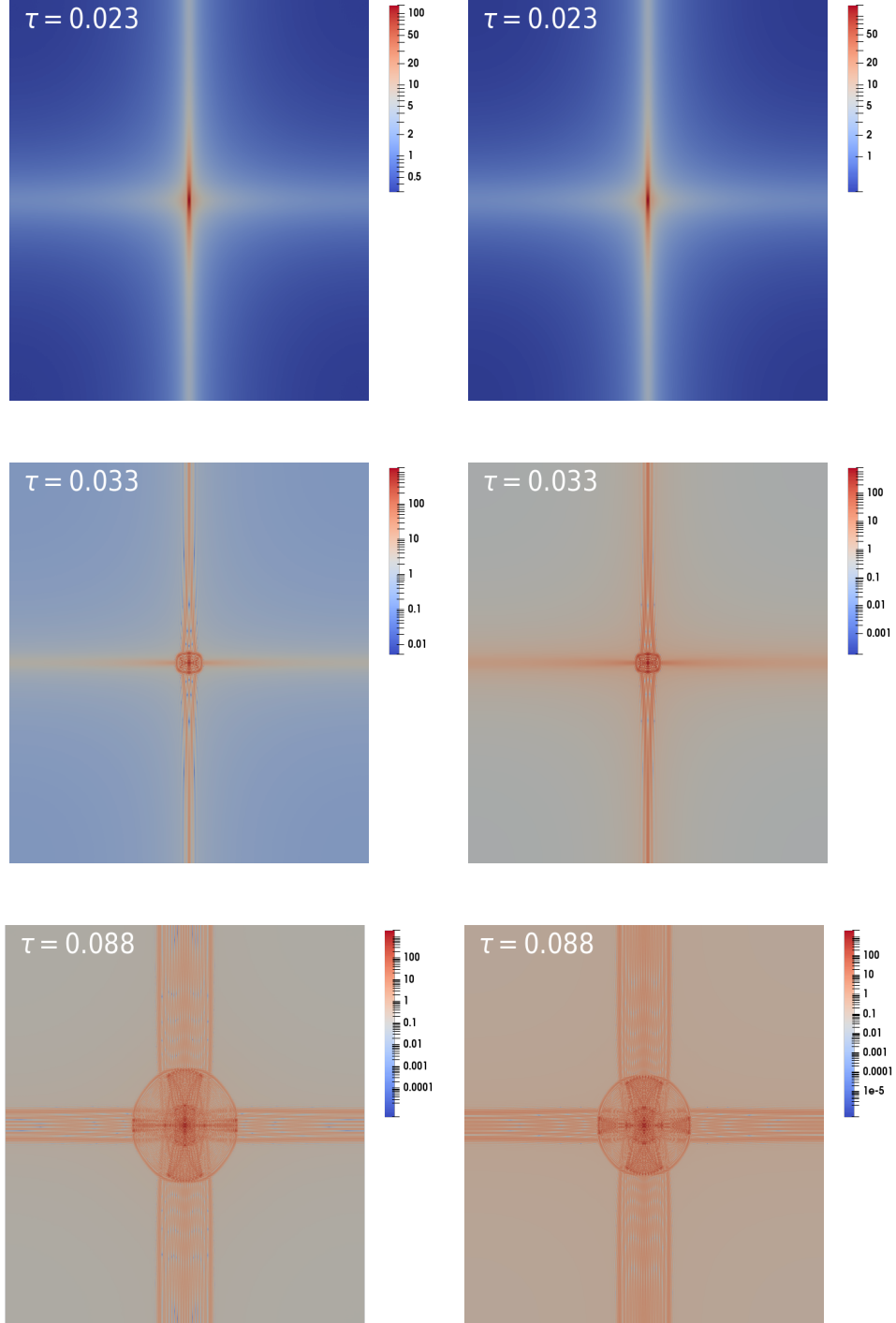


FIGURE 3. The density $|U_h(\tau)|^2$ (logarithmic scale) at $\tau = 0.023$, 0.033 , 0.088 : 1024×1024 grid (left), 2048×2048 grid (right).

- [6] S. Bohun, R. Illner, H. Lange and P.F. Zweifel, *Error estimates for Galerkin approximations to the periodic Schrödinger-Poisson system*, ZAMM Journal of applied mathematics and mechanics Zeitschrift für angewandte Mathematik und Mechanik 1996, 7–13, 1996
- [7] F. Brezzi and P.A. Markowich, *The three-dimensional Wigner-Poisson problem: Existence, uniqueness and approximation*, Math. Methods Appl. Sci. 14, 35–61, 1991
- [8] W. Bao, N. Mauser and H.P. Stimming, *Effective one particle quantum dynamics of electrons: A numerical study of the Schrödinger-Poisson- $X\alpha$ model*, Comm. Math. Sciences. 1, 809–828, 2003.
- [9] P. Bertrand, N. Van Tuan, M. Gros, B. Izrar, M. Feix, and J. Gutierrez, *Classical Vlasov plasma description through quantum numerical methods*, Journal of Plasma Physics, 23(3), 401–422, 1980.
- [10] F. Castella, *L^2 -solutions to the Schrödinger-Poisson system: existence, uniqueness, time behaviour and smoothing effects*, Math. Mod. Meth. Appl. Sci. 7, 1051–1083, 1997
- [11] G. Davies and L. Widrow, *Test-bed simulations of collisionless, self-gravitating systems using the Schrödinger method*, The Astrophysical Journal, 485(2), 1997.
- [12] M. Ehrhardt and A. Zisowsky, *Fast calculation of energy and mass preserving solutions of Schrödinger-Poisson systems on unbounded domains*, Journal of Computational and Applied Mathematics 2006, 187, 1–28, 2006
- [13] R. Illner, P.F. Zweifel and H. Lange, *Global existence, uniqueness and asymptotic behaviour of solutions of the Wigner-Poisson and Schrödinger-Poisson systems*, Math. Meth. Appl. Sci. 17, 349–376, 1994
- [14] S. Jin, H. Wu and X. Yang, *A numerical study of the Gaussian beam methods for Schrödinger-Poisson equations*, J. Comput. Appl. Math. 28, 261–272, 2010.
- [15] Th. Katsaounis and I. Kyza, *A posteriori error analysis for evolution nonlinear Schrödinger equations up to the critical exponent*, SIAM Journal of Numerical Analysis, 56(3), 1405–1434, 2018.
- [16] M. Kopp, K. Vattis and C. Skordis, *Solving the Vlasov equation in two spatial dimensions with the Schrödinger method*, Physical Review D, 96, 123532, 2017.
- [17] C. Lubich, *On splitting methods for Schrödinger-Poisson and cubic nonlinear Schrödinger equations*, Mathematics of Computation 77, 2141–2153, 2008
- [18] T. Lu and W. Cai, *A Fourier spectral-discontinuous Galerkin method for time-dependent 3-D Schrödinger-Poisson equations with discontinuous potentials*, Journal of Computational and Applied Mathematics 220, 588–614, 2008
- [19] P. Markowich, C. Ringhofer and C. Schmeiser, *Semiconductor equations*, Springer, Berlin, 1990
- [20] C. Ringhofer and J. Soler, *Discrete Schrödinger-Poisson systems preserving energy and mass*, Appl. Math. Lett. 13, 27–32, 2000.
- [21] P. Tod and I.M. Moroz, *An analytical approach to the Schrödinger-Newton equations*, Nonlinearity 12, 201–216, 1999.
- [22] C. Uhlemann, M. Kopp, and T. Haugg, *Schrödinger method as N -body double and UV completion of dust*, Phys. Rev. D 90(2), 023517, 2014.
- [23] L. Widrow and N. Kaiser, *Using the Schrödinger equation to simulate collisionless matter*, Astrophysical Journal Letters 416, p.L71, 1993.
- [24] Y. Zhang and X. Dong, *On the computation of ground state and dynamics of Schrödinger-Poisson-Slater system*, J. Comput. Phys. 230, 2660–2676, 2011.
- [25] Y. Zhang, *Optimal error estimates of compact finite difference discretizations for the Schrödinger-Poisson system*, Commun. Commut. Phys., 13, 1357–1388, 2015.
- [26] P. Zhang, Y. Zheng and N. Mauser, *The limit from the Schrödinger-Poisson to the Vlasov-Poisson equations with general data in one dimension*. Communications on Pure and Applied Mathematics. 55, 582 - 632, 2002.

(Agissilaos Athanassoulis) DIVISION OF MATHEMATICS, UNIVERSITY OF DUNDEE, DUNDEE DD1 4HN, SCOTLAND, UK

Email address: a.athanassoulis@dundee.ac.uk

(Theodoros Katsaounis) DEPT. OF MATH. AND APPLIED MATHEMATICS, UNIV. OF CRETE, GREECE & IACM-FORTH, HERAKLION, GREECE

Email address: thodoros.katsaounis@uoc.gr

(Irene Kyza) DIVISION OF MATHEMATICS, UNIVERSITY OF DUNDEE, DUNDEE DD1 4HN, SCOTLAND, UK

Email address: ikyza@maths.dundee.ac.uk

(Stephen Metcalfe) DEPT. OF MECHANICAL ENGINEERING, MCGILL UNIV., MONTREAL, CANADA

Email address: smetcalfehd@gmail.com